CrystEngComm

ROYAL SOCIETY OF CHEMISTRY

PAPER

View Article Online
View Journal

Cite this: DOI: 10.1039/d5ce00079c

Synthon modularity in crystal structure prediction: designing pomalidomide polymorphs and co-crystals†

Zahrasadat Momenzadeh Abardeh, [ab] Alireza Salimi *[a] and Artem R. Oganov *[b]

Received 21st January 2025,
Accepted 30th June 2025

DOI: 10.1039/d5ce00079c

rsc.li/crystengcomm

Synthon modularity is valuable for crystal structure prediction (CSP), allowing for the rationalization of polymorphs and co-crystals. This work used CSP to investigate the crystal structures of the pharmaceutical compound pomalidomide and its co-crystals with urea, gallic acid, and 3,4-dihydroxybenzoic acid (DHBA). By integrating crystal engineering (CE) principles and leveraging the concept of synthon modularity, we identified and characterized two polymorphs of pomalidomide (forms A and B) and proposed its co-crystal structures. Comparative analysis with analogous compounds like thalidomide and lenalidomide revealed shared synthon interactions, supporting the predictive reliability of the approach. These findings highlight the potential of synthon-guided CSP in advancing pharmaceutical crystallography and fostering the development of novel materials.

1 Introduction

Crystal structure plays a crucial role in determining substances' physical and chemical properties, such as stability, melting points, solubility, morphology, *etc.* It is through the understanding of the crystal structure that we can derive properties.[1–3] Predicting and controlling crystal structures of materials is a fundamental aspiration in materials science, chemistry, and pharmaceutical research. **CSP** is a computational approach to predict a molecule's likely crystal structures.[4–7] It generates a list of possible crystal structures, often with tiny energy differences, the latter making it challenging to identify the correct structure.[8,9] In this context, integrating **CSP** with other relevant criteria can aid in pinpointing the precise crystal structure.[10–12] The phenomenon of polymorphism, where a compound can adopt various crystal structures accessible experimentally, further complicates **CSP** calculations.[13–17] When the experimentally observed polymorph is the thermodynamic form, it corresponds to the global free-energy minimum. In **CSP** studies this state is usually approximated by the lowest lattice energy calculated at 0 K. Conversely, when the experimentally observed polymorph is a kinetically stable (metastable) form, its free energy lies above the global minimum. It is crucial to consider both kinetic and thermodynamic factors to identify all potential polymorphs of a molecule.[18] However, today's computational methods mostly address thermodynamic factors with little attention to kinetic factors.[18–20]

Crystal engineering concepts provide a synthon-based screen that helps identify promising crystal structures during **CSP**. They leverage the principles of supramolecular chemistry and non-covalent interactions to manipulate and guide the assembly of molecules into specific crystal structures.[19–21] By understanding the role of molecular motifs and the intricacies of crystal packing, crystal engineering offers a strategic advantage in predicting and designing novel crystal structures.[21] Here, we explore the efficiency of crystal engineering in **CSP** in the case of pomalidomide, a racemic pharmaceutical compound. Pomalidomide, a derivative of thalidomide, finds application in treating cases of multiple myeloma that have relapsed or proven resistant to treatment.[22–24] Classified within the immunomodulation agent drug class, its **IUPAC** name is 4-amino-2-(2,6-dioxopiperidin-3-yl)isoindole-1,3-dione.[25] Fig. 1 depicts the molecular structure of pomalidomide. Although no crystal structure has yet been reported for pomalidomide, several

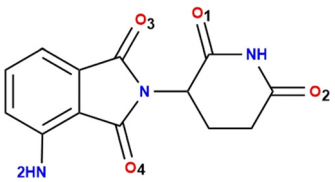

Fig. 1 Chemical structure of pomalidomide, (*R*,*S*)-4-amino-2-(2,6-dioxopiperidin-3-yl)isoindole-1,3-dione, showing the atom numbering for oxygen atoms.

[a] *Department of Chemistry, Faculty of Science, Ferdowsi University of Mashhad, Mashhad, Iran. E-mail: salimi-a@um.ac.ir*
[b] *Skolkovo Institute of Science and Technology, Skolkovo Innovation Center, Moscow 143026, Russian Federation. E-mail: A.Oganov@skoltech.ru*

† Electronic supplementary information (ESI) available. See DOI: https://doi.org/10.1039/d5ce00079c

patents describe a rich solid-form landscape: US10835522B2 (and the earlier US9974780B2) claim forms A and B; WO2018/0099944A1 reports form B again together with a new form M and a gentisic-acid co-crystal; US10093647B1 discloses a crystalline dihydrate; and US20170088537A1 as well as WO2014170909A2 detail the preparation of form I.

The availability of PXRD patterns for these polymorphs, combined with complete crystal structures of closely related thalidomide and lenalidomide derivatives in the **CSD**, provides an excellent platform for testing synthon modularity within our **CSP** workflow. To extend the study to multicomponent systems, we selected urea, gallic acid and 3,5-dihydroxybenzoic acid—the same coformers that have already produced robust lenalidomide cocrystals and markedly improved their apparent solubility and dissolution rate. Using the same coformers allows us to probe whether r identical hydrogen-bond synthons re-emerge in pomalidomide and whether comparable property gains can be realised, while simultaneously assessing the effectiveness of crystal engineering concepts in guiding **CSP**.

One of the primary challenges in **CSP** is the ranking and selection of crystal structures from a vast array of possible crystal structures.[26,27] The energy landscape of crystals is intricate and influenced by a delicate balance of various interactions. The likelihood of a particular crystal structure to emerge in an experiment depends on an interplay of thermodynamic and kinetic factors.[28] To address this challenge, crystal engineering introduces the concept of synthons, intermolecular interactions acting like 'building blocks' or 'glue' between molecules, holding them together within a crystal structure.[21] Synthon interactions often reappear in compounds that share common molecular components, a phenomenon we refer to as synthon modularity.[29,30] Put simply, if a specific synthon interaction (X) is observed repeatedly in several known derivatives within a molecular family, there is a strong likelihood that the same synthon interaction will appear in the next, as-yet-unknown member of that family.

This concept is practically useful because identifying recurring synthon interactions in known compounds helps to predict their occurrence in structurally similar but unknown compounds, even when other intermolecular interactions are difficult to predict. In our study, this insight proved effective as a practical tool for screening and selecting structures generated during **CSP** runs. Hence, recognising synthon modularity offers a promising route for ranking and selecting candidate crystal structures within **CSP**. Throughout this work we use standard graph-set notation to describe hydrogen-bond patterns; for example, $R_2^2(8)$ denotes an eight-membered ring formed by two hydrogen-bond donors and two hydrogen-bond acceptors.[31,32]

Co-crystals, another intriguing aspect of crystal engineering, open doors to new applications of **CSP**.[33–35] These hybrid crystalline materials comprise two or more distinct molecular components held together by non-covalent interactions. Co-crystals offer a versatile platform for tailoring the properties of materials by combining active pharmaceutical ingredients with suitable coformers.[36,37] Predicting and designing co-crystals is an evolving field within **CSP**, where crystal engineering principles are invaluable.[38]

Studying the stability of co-crystal structures with different ratios of components is challenging. Rigorously, thermodynamic stability is quantified by the convex hull construction and d_h, the energy above the convex hull.[39,40]

The convex hull diagram, which plots the free energy of formation $\Delta G_{(A_xB_y)}$ against the compositions, illustrates how this energy varies with different stoichiometric ratio of co-crystals. Structures lying on the convex hull are more thermodynamically stable than those not on the convex hull, and d_h reflects its degree of stability or metastability relative to the most stable structures on the convex hull. We utilized d_h as a criterion for ranking the predicted co-crystal structures.

Analysis of **CSD** provides a wealth of experimental data that can be harnessed to validate and improve **CSP** results.[10–12] By comparing predicted structures with those found in the **CSD**, researchers can refine their computational models and enhance the accuracy of their predictions. This article investigates the utilization of crystal engineering concepts such as the synthon approach and synthon modularity within **CSP**. The central question of this study is whether the concept of synthon modularity, based on the repeatable and transferable hydrogen bonding patterns observed in thalidomide and lenalidomide structures, can help reduce the complexity of **CSP** for pomalidomide, a compound with no reported crystal structure but with known PXRD patterns from patents.

2 Computational methodology

The geometry of all molecular structures was optimized by density functional theory (DFT), using Gaussian 09 program[41] B3LYP hybrid functional and 6-311g(p,d) basis set. The evolutionary algorithm USPEX was used to search for low-energy structures.[42–45]

2.1 Conformational search

The conformational search was done using the Dreiding force field,[46] with atomic charges determined by atomic-Qeq[47] (Fig. S1†). A **CSD** search (**CSD** version 5.38, updated November 2021) was conducted to analyze the torsion angle distribution in the similar molecular structures. The corresponding results are in Fig. S2 (ESI†).

2.2 Generation of structures

Pomalidomide. Each generation in the USPEX computations had 120 structures. The first generation was produced using a random symmetric structure generator within the most common racemic space groups $P\bar{1}$, $P2_1/c$, $Pbca$, $C2/c$, Cc, Pc, $Pna2_1$, $Pnma$, and $Pca2_1$, and one molecule in the asymmetric unit ($Z' = 1$). The lowest-energy 60% of the

generated structures were used as parents to produce subsequent generations. The second and subsequent generations comprised 100 structures produced by variation operators (50% by heredity, 10% by softmutation, and 10% by rotational mutation), with a random symmetric structure generator producing 30% of the generation. At T = 0 K and ambient pressure, the energy of all generated structures was used as fitness. All structures were optimized using the GULP code[48]/Dreiding force field[46] (atomic charges_Qeq[47]). To ensure that synthon-rich packings were not discarded as parents by the approximate Dreiding energy, every five to six generations all structures were inspected in Mercury; any packing displaying at least one target synthon was injected back as seed for the next generation. At the post-processing step, we selected low-energy structures, removed duplicate structures (identified using the packing similarity search in Mercury software based on RMSD15 criteria)[49] and reoptimized all structures using the PBE–D3[50] method as implemented in VASP[51–53] within the framework of the projector augmented wave (PAW) method.[54,55] The kinetic energy cutoff of 700 eV, Brillouin zone sampling with a k-point grid of $2\pi \times 0.06$ Å^{-1} resolution, and convergence criteria of 1×10^{-5} eV per atom for total energies and 5×10^{-3} eV Å^{-1} for forces were used.

2.3 Free energy and convex hull analysis of co-crystals

To evaluate the thermodynamic stability of predicted co-crystal structures, we constructed convex hull diagrams based on the Gibbs free energy of formation for each stoichiometry. Structure generation was performed for various stoichiometric ratios of pomalidomide to coformer, including 1 : 1, 1 : 2, 2 : 1, 2 : 3, and 3 : 2. The Gibbs free energy of each co-crystal structure was computed as:

$$G = E_{\mathrm{VASP}} + F_{\mathrm{vib}}(298.15\ \mathrm{K}) + PV$$

where E_{VASP} is the total lattice energy obtained from periodic DFT optimization using the PBE-D3 functional in VASP, F_{vib} (298.15 K) is the vibrational (Helmholtz) free energy at 298.15 K, computed *via* phonon calculations in GULP using the GFN-FF[56] force field, PV is the pressure–volume term. P is pressure and V is volume, and under ambient conditions, the PV term is negligible for solids.

This hybrid approach allowed us to incorporate temperature-dependent corrections efficiently while retaining the accuracy of DFT lattice energies. The Gibbs free energy of formation for each co-crystal was then calculated per molecule using:

$$\Delta G_{(\mathrm{A}_x\mathrm{B}_y)} = \frac{G_{(\mathrm{A}_x\mathrm{B}_y)} - xG_{\mathrm{A}} - yG_{\mathrm{B}}}{x+y}$$

where G_{A} and G_{B} represent the Gibbs free energies of the pure components A (pomalidomide) and B (coformer), respectively. The convex hull was constructed by plotting $\Delta G_{(\mathrm{A}_x\mathrm{B}_y)}$ against the composition, which was defined as:

$$\mathrm{Composition} = Z_1/(Z_1 + Z_2)$$

where Z_1 and Z_2 represent the number of pomalidomide and coformer molecules in the unit cell, respectively. Each co-crystal appears as a point on this plot. The parameter d_{h} is defined as the shortest vertical distance from that point to the convex hull. It measures how far a structure is from thermodynamic stability. Structures that lie on the convex hull (d_{h} = 0.00 kJ mol^{-1}, per molecule) are thermodynamically stable. Structures above the convex hull have positive d_{h} and are considered metastable. Therefore, we ranked all predicted co-crystal structures based on their d_{h} values, and the most stable ones were further evaluated in terms of synthon modularity.

Using Gibbs free energies instead of lattice energies improved the thermodynamic accuracy of our predictions, especially for systems where temperature effects are significant. This combined VASP–GULP protocol enabled reliable and efficient screening of co-crystal candidates while keeping computational cost low.

3 Results and discussion

3.1 Synthon modularity

Based on the available knowledge about compounds similar to pomalidomide, the concept of synthon modularity can be utilized to select the generated structures in the crystal structure prediction of this pharmaceutical molecule. Fig. 2 shows an interesting structural connection between thalidomide, pomalidomide, lenalidomide, and phthalimidine.

Fig. 2 shows that by adding an amino group to phthalimidine and thalidomide molecules, they become lenalidomide and pomalidomide molecules, respectively. Also, by adding a carbonyl group to lenalidomide and phthalimidine, pomalidomide and thalidomide are obtained,

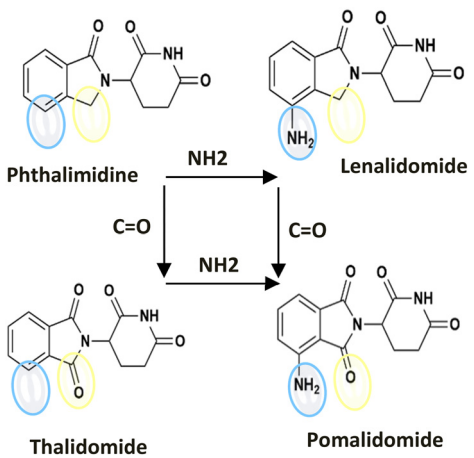

Fig. 2 Structural relationships among thalidomide derivatives and the concept of synthon modularity in crystal structure prediction. 2D molecular structures of phthalimidine, thalidomide, lenalidomide, and pomalidomide. Vertical arrows (top to bottom) indicate the addition of a carbonyl group, while horizontal arrows (left to right) show the addition of an amine group at equivalent substitution sites.

respectively. All compounds include the $R_2^2(8)$ synthon. This synthon connects molecules through strong NH···O hydrogen bonds between imide groups. We expect that the interactions observed for the carbonyl groups related to thalidomide derivatives, and the amine groups in the crystal and co-crystals of lenalidomide would also be observed in the corresponding functional groups of pomalidomide.

The behavior of the amine group interaction. The amine group may form N–H···O hydrogen bonds with four carbonyl oxygen atoms in the molecular structure. Determining which oxygen atom is most likely to participate in the N–H···O interaction can be beneficial when selecting potential polymorphs. Therefore, investigating the interaction behavior of the amine group within the crystal and co-crystal structures of lenalidomide, with a focus on synthon modularity, can provide insights into this phenomenon. Lenalidomide exhibits two polymorphs and three co-crystals with **CSD** reference codes AJISES,[57] AJISES01,[58] XODPOX,[59] HUVGAI,[60] and XODPIR,[59] crystallizing in the space groups $P\bar{1}$, *Pbca*, $P2_1/c$, $P\bar{1}$, and $P\bar{1}$, respectively. In all of these structures, the amine group participates in an N–H···O hydrogen bond interaction with imide carbonyls, as illustrated by **Syn I** (dark blue, Fig. 3a).

The interaction behavior of the carbonyl group. In Fig. 1, the oxygen atoms of the pomalidomide molecule are labelled. The interaction behavior of oxygen atom 3 (found in all thalidomide derivatives) and oxygen atom 4 (common in both thalidomide and pomalidomide) were investigated in thalidomide derivatives. A comprehensive **CSD** search was conducted to identify polymorphs of thalidomide without imposing any error, polymeric, or ion-related restrictions. As a result, four distinct polymorphs were found, denoted as THALID03,[61] THALID10,[62] THALID11,[63] and THALID12,[64] each associated with the $C2/c$, $P2_1/n$, $C2/c$, and $P2_1/n$ space groups, respectively. It is noteworthy that the C–H···O interaction between oxygen atom 4 and aromatic C–H (C_6-ring) is a common feature observed in all thalidomide polymorphs, which is represented as **Syn II** (depicted in green in Fig. 3a). In certain thalidomide derivatives, such as phthalimidine, the hydrogen bond interaction forms a dimer synthon, denoted as $R_2^2(10)$, involving oxygen atom 3 and hydrogen atom 6.

In other cases, the imide NH group and oxygen atom 3 engage in NH···O hydrogen bonding interactions (colored in purple in Fig. 3a), identified as **Syn III**. As Fig. 3(b) demonstrates, based on the synthon modularity concept, it is anticipated that **Syn I**, **Syn II**, and **Syn III** will also be observed in the polymorphs of pomalidomide. The observed synthons in all experimental structures are shown in Fig. S3 (ESI†).

Synthon modularity in co-crystals. The co-crystal of lenalidomide with urea was crystallized in a 1 : 1 ratio within the monoclinic crystal system and the space group $P2_1/c$ (XODPOX[59]). In this structure, the imide group, when combined with urea, forms the hetero-synthon $R_2^2(8)$. Furthermore, the homo-synthon $R_2^2(8)$ emerges from the interaction between two urea molecules, facilitating the connection of two synthon $R_2^2(8)$. These intricate interactions are highlighted in Fig. 4.

Lenalidomide and gallic acid were co-crystallized in a 1 : 1 ratio within the space group $P\bar{1}$ (HUVGAI[60]). Fig. 4 provides synthon interactions in the molecular packing in this co-crystal. Here, an NH···O hydrogen bond is established between the imide group and the carbonyl group of the acid. Additionally, the hetero-synthon $R_2^2(9)$ is formed through interactions between gallic acid and the imide group (as depicted in Fig. 6). Notably, OH···O hydrogen bonding is observed between the carbonyl group of lenalidomide and the O–H and C–H groups of **GA**.

The co-crystal of lenalidomide with **DHBA**, in a 1 : 1 ratio and within the $P\bar{1}$ space group (XODPIR[59]), is also known from experiment. As demonstrated in Fig. 4, the molecular arrangement features molecular tetramers composed of two hetero-synthons, $R_2^2(8)$ and $R_2^2(12)$. These tetramers are interconnected through hydrogen bonding homo-synthons $R_2^2(8)$ established between two **DHBA** molecules.

3.2 Molecular conformational analysis

The pomalidomide molecule features an amine substitution, a torsion angle, and a chiral carbon, enabling the molecule to

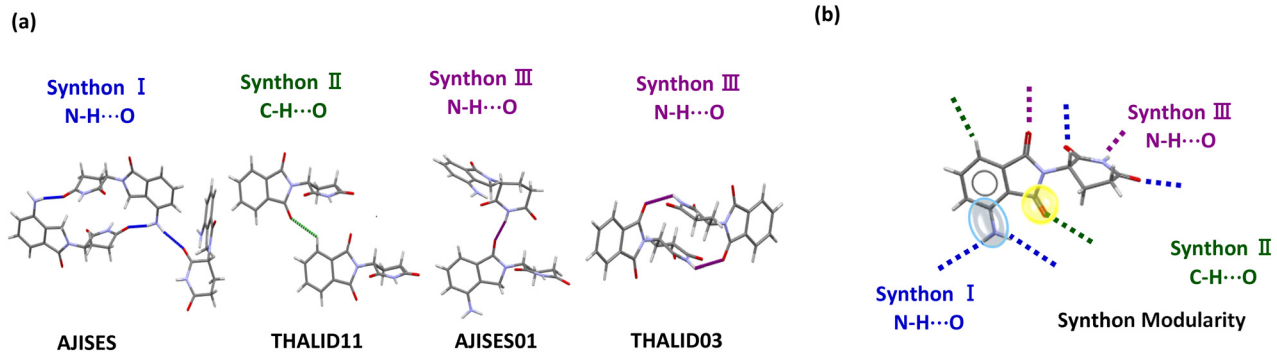

Fig. 3 (a) Common synthons in known crystal structures of thalidomide (THALID11, THALID03) and lenalidomide (AJISES, AJISES01). The synthons and interactions are identified clearly by color and labeling: synthon I (N–H···O, blue), synthon II (C–H···O, green), and synthon III (N–H···O, purple). (b) Anticipated synthons and interactions for pomalidomide based on the synthon modularity concept, shown in positions analogous to those observed in thalidomide and lenalidomide. Colors and labels correspond to those established in part (a).

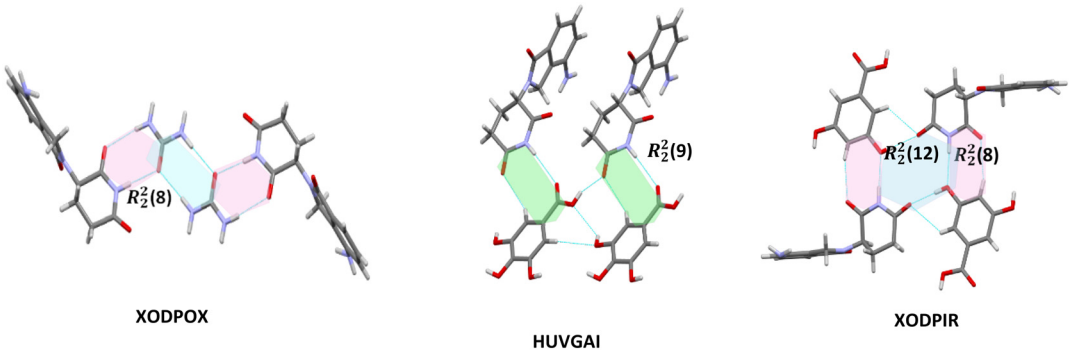

Fig. 4 Synthon interactions in the co-crystals of lenalidomide are shown as follows: with urea—$R_2^2(8)$ hetero-synthon in pink and $R_2^2(8)$ homo-synthon in blue; with gallic acid—$R_2^2(9)$ hetero-synthon in green; and with **DHBA**—$R_2^2(8)$ in pink and $R_2^2(12)$ in blue.

exist in multiple conformational states. These features were investigated by examining the observed conformational states of thalidomide derivatives. Thalidomide derivatives share common characteristics in their molecular structures, such as the coplanarity of the CH chiral group with the five-membered ring. Torsion angle computations were performed using the Dreiding force field (Qeq) to explore various conformational states. The results, illustrated in Fig. S1,† reveal three conformational states. These findings align with the torsion angle analysis conducted in the **CSD** search (Fig. S2†). The energy gap between conformers 1 and 2 is only 0.37 kJ mol^{-1} (Table S1†). All reported crystal and co-crystal structures of lenalidomide—a molecule that differs from pomalidomide by only one carbonyl group—adopt the geometry corresponding to conformer 2, which readily accommodates the CH···O hydrogen-bond synthon II, a motif common to thalidomide derivatives. We therefore selected conformer 2 as the starting point for **CSP**.

3.3 Crystal structure prediction

3.3.1 CSP calculation of pomalidomide. In the **CSP** calculation, approximately 12 000 structures were generated.

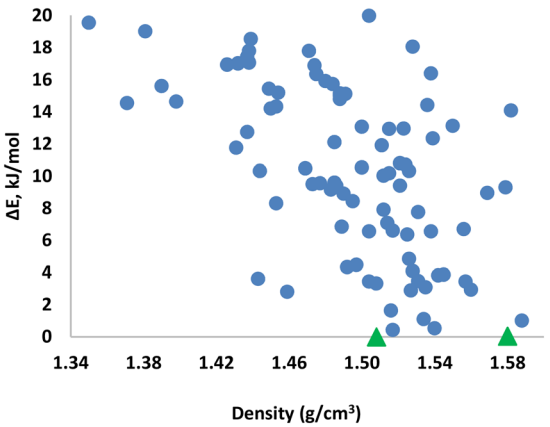

Fig. 5 Lattice energy (ΔE, PBE-D3, kJ mol^{-1}) relative to the ground state plotted against the density for the generated structures of pomalidomide. Selected structures, based on synthon modularity, are highlighted in green.

The entire low-energy set that lay below the Dreiding cut-off (40 kJ mol^{-1}) was selected for DFT optimization after duplicates had been removed (RMSD15 = 0.2 Å). Structures above this threshold were screened in Mercury; any packing that contained at least one target synthon was added to the selection. In total, 195 unique structures were retained, whose crystallographic data are listed in ESI† Table S2. All selected structures were then optimized in VASP with the PBE-D3 method and ranked by lattice energy.

Fig. 5 depicts the PBE-D3 energy against the density of the generated structures, and the low-energy structures within 5 kJ mol^{-1} of the most stable generated structure are presented in Table 1. Analysis of the generated structures reveals that their key distinguishing feature is synthon. Pomalidomide molecules consist of imide, amine, carbonyl, and CH groups. Considering these interaction sites, strong hydrogen bonds (NH···O) can play a crucial role in assembling pomalidomide polymorphs. It is essential to understand the geometry of these synthons and where they are most likely to occur. In this context, the results of the **CSD** search based on synthon modularity were utilized.

Given the synthon modularity observed in experimental structures (section 3.1), we anticipate that **Syn I**, **Syn II**, and **Syn III** synthons (Fig. 3) will also be present in pomalidomide polymorphs. The generated structures were analyzed in terms of synthon modularity, and Table 1 indicates the presence (Y) or absence (N) of synthons **Syn I**, **Syn II**, and **Syn III** for each structure. Remarkably, as anticipated, the top-ranked structures (1 and 2) include all three synthons. Powder X-ray diffraction and synthon interactions of ranks 1 and 2 are shown in Fig. 6. The relative energy difference between ranks 1 and 2 is negligible, approximately 0.05 kJ mol^{-1}. In Fig. 6, the simulated diffraction patterns of rank 1 and rank 2 structures are compared with the reported diffraction patterns for the experimental polymorphs in the patent.[65] The results demonstrate that the predicted structures of ranks 1 and 2 match polymorphs B and A, respectively (Table 2). These results underscore the value and efficiency of crystal engineering concepts in identifying potential structures among the predicted ones.

3.3.2 CSP calculation of co-crystals. In the **CSP** of co-crystals, stoichiometric ratios of 1 : 1, 1 : 2, 2 : 1, 2 : 3, and 3 :

Table 1 Pomalidomide structures within 5 kJ mol^{-1} of the most stable generated structure, indicating the presence (Y) or absence (N) of synthons **Syn I**, **Syn II**, and **Syn III** for each generated structure

Rank	Space group	Z	Volume per molecule, Å^3	Density, g cm^{-3}	ΔE, kJ mol^{-1}	**Syn I**	**Syn II**	**Syn III**
1	***P*$\bar{1}$**	**2**	**300.87**	**1.51**	**0.00**	**Y**	**Y**	**Y**
2	***P*$\bar{1}$**	**2**	**287.22**	**1.58**	**0.05**	**Y**	**Y**	**Y**
3	*P*$\bar{1}$	2	299.16	1.52	0.43	Y	Y	N
4	*P*$\bar{1}$	2	294.66	1.54	0.53	Y	Y	N
5	*P*$\bar{1}$	2	285.69	1.59	1.01	Y	Y	N
6	*P*$\bar{1}$	2	295.77	1.53	1.11	Y	Y	N
7	*P*$\bar{1}$	2	299.27	1.52	1.64	N	N	N
8	*Pbca*	8	310.91	1.46	2.81	Y	N	Y
9	$P2_1/c$	4	297.04	1.53	2.89	Y	Y	N
10	*P*$\bar{1}$	2	290.82	1.56	2.94	Y	N	Y
12	$P2_1/c$	4	300.93	1.51	3.33	Y	N	N
13	$P2_1/c$	4	301.64	1.50	3.45	Y	N	N
14	*C*2/*c*	8	291.51	1.56	3.45	Y	Y	N
15	*P*$\bar{1}$	2	296.39	1.53	3.47	Y	N	Y
16	$P2_1/c$	4	314.38	1.44	3.62	N	N	N
17	*C*2/*c*	8	294.34	1.54	3.82	Y	Y	N
18	*C*2/*c*	8	293.62	1.55	3.87	Y	Y	N
19	*Pbca*	8	296.95	1.53	4.10	Y	N	Y
20	$P2_1/c$	4	304.15	1.49	4.34	Y	Y	N

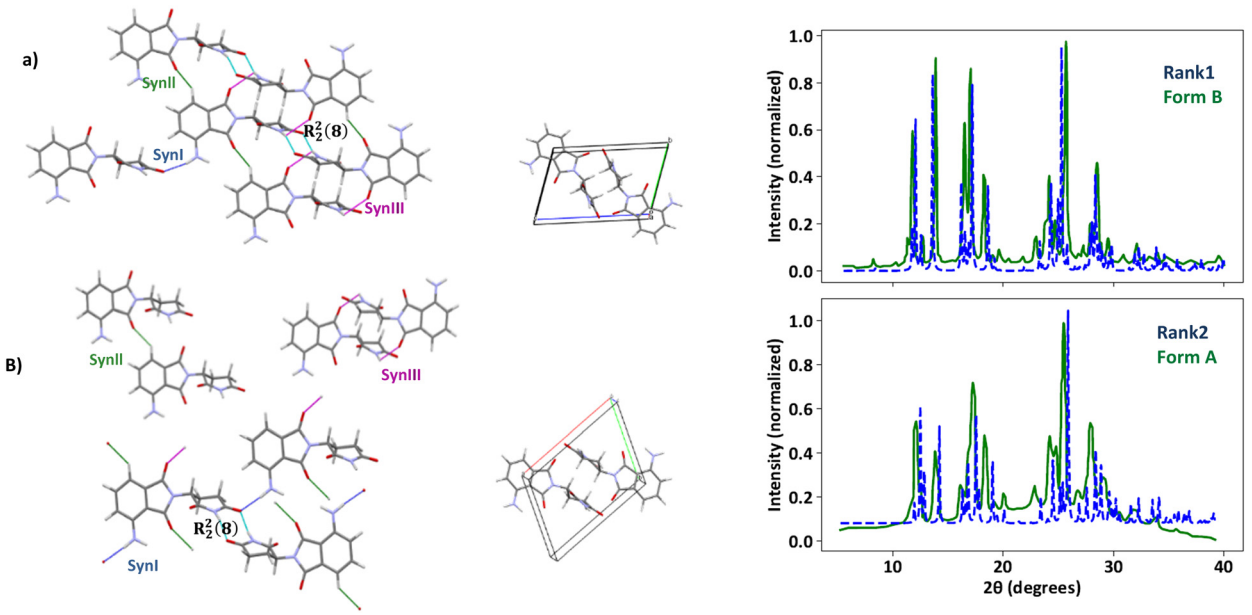

Fig. 6 Crystal structures, synthon interactions, and powder X-ray diffraction patterns (λ = 1.54° A) for rank 1 and rank 2 structures. The experimental PXRD patterns of pomalidomide polymorphs (form B and form A)[65] are shown as solid green lines, while the calculated patterns for the predicted structures (rank 1 and rank 2) are displayed as dashed blue lines after applying optimal shifts of 0.46° and 0.30°, respectively. Similarity between patterns was quantitatively assessed using the FIDEL method,[66] yielding optimal shifts of 0.46° for form B and 0.3° for form A, with similarity scores (S_{12}) of 0.7658 and 0.8058, respectively.

2 were considered. Separate **CSP** runs were conducted for each ratio. A significant number of structures were generated, and after removing high-energy, low-density, and duplicate structures (RMSD = 0.2 Å), the remaining structures were re-optimized using VASP with the PBE-D3 functional. The Gibbs free energy of co-crystal formation, $\Delta G_{(A_xB_y)}$, was calculated to evaluate the potential for co-crystal formation. Convex hull plots were then constructed to identify thermodynamically stable stoichiometries, as shown in Fig. 7.

CSP of co-crystal of pomalidomide with urea. Altogether, more than 50 000 structures were generated across all stoichiometric ratios. After removing high-energy, low-density, and duplicate structures (RMSD = 0.2 Å), a total of 850 structures remained and were re-optimized using VASP with the PBE-D3 functional. The Gibbs free energy of formation,

Table 2 The unit cell parameters of the experimental form A and the predicted structures in rank 1 and 2 (for form B the unit cell parameters were not reported in the patents)

Rank	SPG	a, Å	b, Å	c, Å	α, °	β, °	γ, °	V, Å^3	g cm^{-3}
Exp./formB[65]	$P\bar{1}$	7.047(9)	7.891(27)	11.310(6)	73.249(13)	80.919(9)	88.596(6)	594.618(8)	1.53
Rank-1	$P\bar{1}$	7.209	7.964	11.357	70.939	77.508	86.328	601.678	1.51
Rank-2	$P\bar{1}$	6.977	7.723	11.278	73.389	80.68	86.009	574.474	1.58

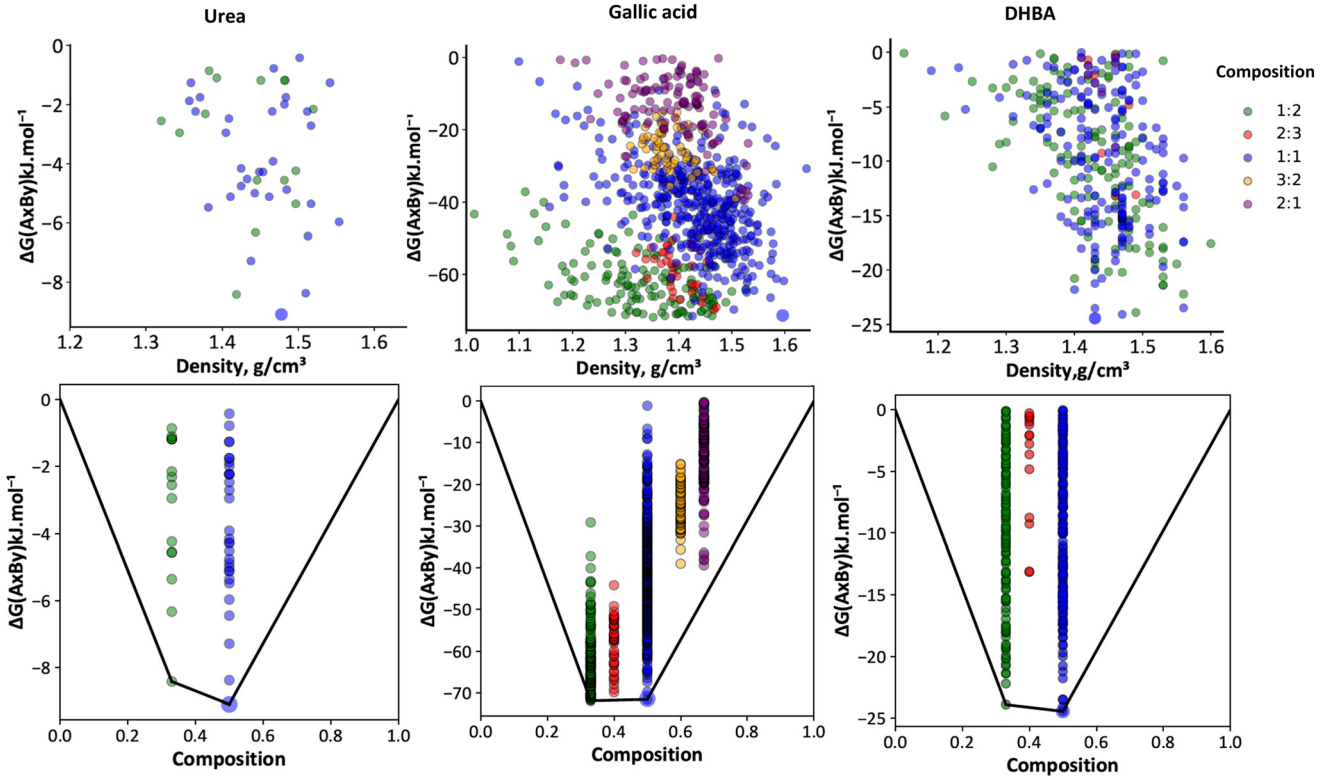

Fig. 7 Convex hull and energy landscape plots of pomalidomide co-crystals with urea, gallic acid, and **DHBA**. Suggested structures based on synthon modularity are size-highlighted.

$\Delta G_{(A_xB_y)}$, was calculated for all structures to evaluate their thermodynamic feasibility (see section 2.3). A large number of co-crystals exhibited positive ΔG values and were therefore excluded. Ultimately, 47 structures with negative Gibbs formation energies were retained for further analysis. These structures were ranked using the d_h parameter. Fig. 7 shows the convex hull and energy landscape plots of the generated co-crystals. Table 3 presents the d_h and $\Delta G_{(A_xB_y)}$ values (in kJ mol^{-1}) for the ten most stable structures. The complete list is provided in the ESI† (Table S3).

Table 3 List of the first 10 generated co-crystal structures of pomalidomide with urea, ranked by d_h. Gibbs free energies of formation (ΔG) were computed using a hybrid DFT (VASP, PBE-D3) and vibrational correction (GULP, GFN-FF). The suggested structure based on synthon modularity is shown in bold

Rank-d_h	Z_1	Z_2	Composition	Volume, Å^3 per asymmetric unit	Density, g cm^{-3}	Space group	$\Delta G_{(A_xB_y)}$ kJ mol^{-1}, per molecule	d_h kJ mol^{-1}, per molecule
1	**4**	**4**	**0.50**	374.50	**1.48**	$P2_1/c$	**−9.10**	**0.00**
2	2	4	0.33	460.30	1.42	$P\bar{1}$	−8.42	0.00
3	4	4	0.50	366.46	1.51	$P2_1/c$	−8.38	0.72
4	4	4	0.50	384.94	1.44	$P2_1/c$	−7.29	1.81
5	2	4	0.33	452.50	1.44	$P\bar{1}$	−6.33	2.09
6	4	4	0.50	365.73	1.51	$P2_1/c$	−6.45	2.65
7	2	4	0.33	436.20	1.50	$P\bar{1}$	−5.36	3.06
8	4	4	0.50	356.13	1.55	$P2_1/c$	−5.97	3.13
9	4	4	0.50	400.51	1.38	$P2_1/c$	−5.48	3.62
10	4	4	0.50	364.88	1.52	$P2_1$/c	−5.36	3.74

CSP of co-crystal of pomalidomide with gallic acid. Approximately 10 000 structures were generated. After filtering out high-energy, low-density, and duplicate structures, 836 candidates were retained and re-optimized using VASP with the PBE-D3 functional. The Gibbs free energy of formation, $\Delta G_{(A_xB_y)}$, was calculated for all structures. Among them, 793 structures exhibited negative ΔG values and were used for convex hull analysis and thermodynamic ranking based on the d_h parameter. The convex hull plot revealed that 1 : 1 and 1 : 2 stoichiometries lie on the hull line, suggesting they are the most thermodynamically favorable compositions. Other ratios, including 2 : 1, fall above the convex hull and are therefore less stable. The energy landscape and convex hull diagram are shown in Fig. 7. The d_h and $\Delta G_{(A_xB_y)}$ values (in kJ mol^{-1}) for the ten most stable co-crystal structures are listed in Table 4. The complete list is provided in the ESI† (Table S4).

CSP of co-crystal pomalidomide with DHBA. In this **CSP** study, approximately 11 600 structures were generated. After filtering out high-energy, low-density, and duplicate entries, 810 structures were re-optimized using VASP with the PBE-D3 functional. The Gibbs free energy of formation, $\Delta G_{(A_xB_y)}$, was calculated for each structure. Among them, 333 exhibited negative ΔG values. To assess their relative stability, a convex hull diagram was constructed, and the corresponding energy landscape is shown in Fig. 7. The analysis revealed that the 1 : 1 and 1 : 2 stoichiometries lie directly on the convex hull, indicating that these are the most likely candidates for experimental realization. The structures were ranked based on the d_h. Table 5 reports the d_h and $\Delta G_{(A_xB_y)}$ values (in kJ mol^{-1}) for the ten most stable co-crystals. These top-ranking structures are further evaluated in terms of synthon modularity in the following section. The complete list is provided in the ESI† (Table S5).

3.4 Synthon modularity in the co-crystals of pomalidomide

Based on synthon modularity, the likely co-crystals were the following:

Co-crystals with urea. The co-crystal structure ranked first, with a 1 : 1 stoichiometry and belonging to the $P2_1/c$ space group, showed the closest synthon correspondence to the known experimental co-crystal of lenalidomide with urea (XODPOX). Both structures exhibit the same hydrogen-bonding motifs, including the hetero-synthon $R_2^2(8)$ between imide and urea groups, and the homo-synthon $R_2^2(8)$ between two urea molecules. As shown in Fig. 8, these interaction patterns are well preserved and clearly comparable between the experimental and predicted structures. Due to its d_h value of 0.00 kJ mol^{-1} and strong synthon match, the rank 1 structure is suggested as the most likely pomalidomide–urea co-crystal.

Table 4 List of the first 10 generated co-crystal structures of pomalidomide with gallic acid, ranked by d_h. Gibbs free energies of formation (ΔG) were computed using a hybrid DFT (VASP, PBE-D3) and vibrational correction (GULP, GFN-FF). The suggested structure based on synthon modularity is shown in bold

Rank-d_h	Z_1	Z_2	Composition	Volume, Å^3 per asymmetric unit	Density, g cm^{-3}	Space group	$\Delta G_{(A_xB_y)}$ kJ mol^{-1}, per molecule	d_h kJ mol^{-1}, per molecule
1	2	4	0.33	753.71	1.35	$P\bar{1}$	−71.91	0.00
2	2	2	0.50	516.27	1.43	$P\bar{1}$	−71.59	0.00
3	**2**	**2**	**0.50**	**461.39**	**1.60**	***P*$\bar{1}$**	**−71.41**	**0.18**
4	2	4	0.33	718.54	1.42	$P\bar{1}$	−71.65	0.26
5	2	4	0.33	696.35	1.46	$P\bar{1}$	−71.52	0.39
6	2	4	0.33	741.61	1.37	$P\bar{1}$	−71.51	0.40
7	2	4	0.33	783.69	1.30	$P\bar{1}$	−71.21	0.70
8	2	4	0.33	728.45	1.40	$P\bar{1}$	−71.05	0.86
9	2	4	0.33	730.28	1.40	$P\bar{1}$	−71.02	0.89
10	2	4	0.33	764.51	1.33	$P\bar{1}$	−71.01	0.90

Table 5 List of the first 10 generated co-crystal structures of pomalidomide with **DHBA**, ranked by d_h. Gibbs free energies of formation (ΔG) were computed using a hybrid DFT (VASP, PBE-D3) and vibrational correction (GULP, GFN-FF). The suggested structure based on synthon modularity is shown in bold

Rank-d_h	Z_1	Z_2	Composition	Volume, Å^3 per asymmetric unit	Density, g cm^{-3}	Space group	$\Delta G_{(A_xB_y)}$ kJ mol^{-1}, per molecule	d_h kJ mol^{-1}, per molecule
1	**2**	**2**	**0.50**	**495.97**	**1.43**	***P*$\bar{1}$**	**−24.43**	**0.00**
2	2	2	0.50	481.49	1.47	$P\bar{1}$	−24.07	0.36
3	2	4	0.33	646.09	1.49	$P\bar{1}$	−23.89	0.00
4	2	2	0.50	497.14	1.43	$P\bar{1}$	−23.51	0.92
5	2	2	0.50	454.41	1.56	$P\bar{1}$	−23.47	0.96
6	2	4	0.33	617.59	1.56	$P\bar{1}$	−22.20	1.69
7	2	2	0.50	508.23	1.40	$P\bar{1}$	−21.78	2.65
8	2	4	0.33	630.45	1.53	$P\bar{1}$	−21.38	2.51
9	2	4	0.33	631.98	1.53	$P\bar{1}$	−21.38	2.51
10	2	2	0.50	497.96	1.43	$P\bar{1}$	−21.22	3.21

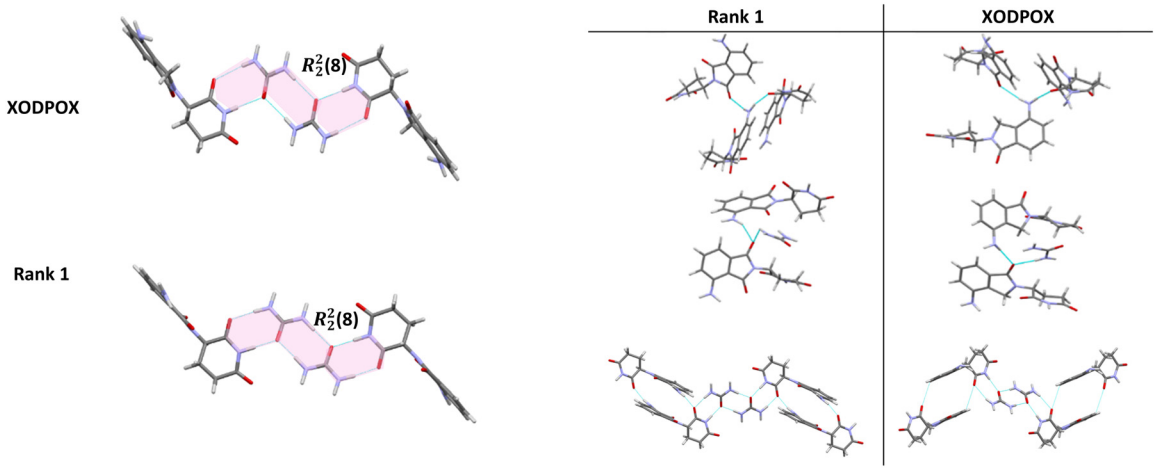

Fig. 8 Synthon interactions for XODPOX (corresponding lenalidomide co-crystal) and the predicted co-crystal of pomalidomide with urea for ranks 1. Comparison of the XODPOX co-crystal with rank 1 in terms of interactions involving amine, imide, and carbonyl groups.

Co-crystals with gallic acid. All ten top-ranked co-crystal structures were examined in terms of synthon modularity. Among them, the rank 3 structure, with a 1:1 stoichiometry and belonging to the $P\bar{1}$ space group, showed the closest match to the known experimental co-crystal of lenalidomide with gallic acid. This structure reproduces the key hydrogen-bonding motifs observed in the experimental counterpart, including the $R_2^2(8)$ hetero-synthon between the imide and acid groups, as well as additional hydrogen bonds involving amino, carbonyl, and hydroxyl groups. These interactions are illustrated and compared in Fig. 9 with a d_h value of 0.18 kJ mol^{-1}. The rank 3 structure is suggested as the most likely pomalidomide–gallic acid co-crystal based on synthon modularity.

Co-crystal with DHBA. The top-ranked co-crystal structures of pomalidomide with **DHBA** were analyzed in terms of synthon modularity. Among them, the rank 1 structure, with a 1:1 stoichiometry and belonging to the $P\bar{1}$ space group, exhibited the strongest correspondence with the experimental co-crystal of lenalidomide with **DHBA** (XODPIR), as illustrated in Fig. 10. The predicted structure reproduces the key supramolecular features observed in XODPIR, including similar stacking arrangements and hydrogen-bonding patterns. Given its d_h value of 0.00 kJ mol^{-1} and strong synthon match, the rank 1 structure is suggested as the most likely pomalidomide–**DHBA** co-crystal.

4 Conclusions

In this study, we used crystal structure prediction (**CSP**) to explore the polymorphic forms and co-crystals of

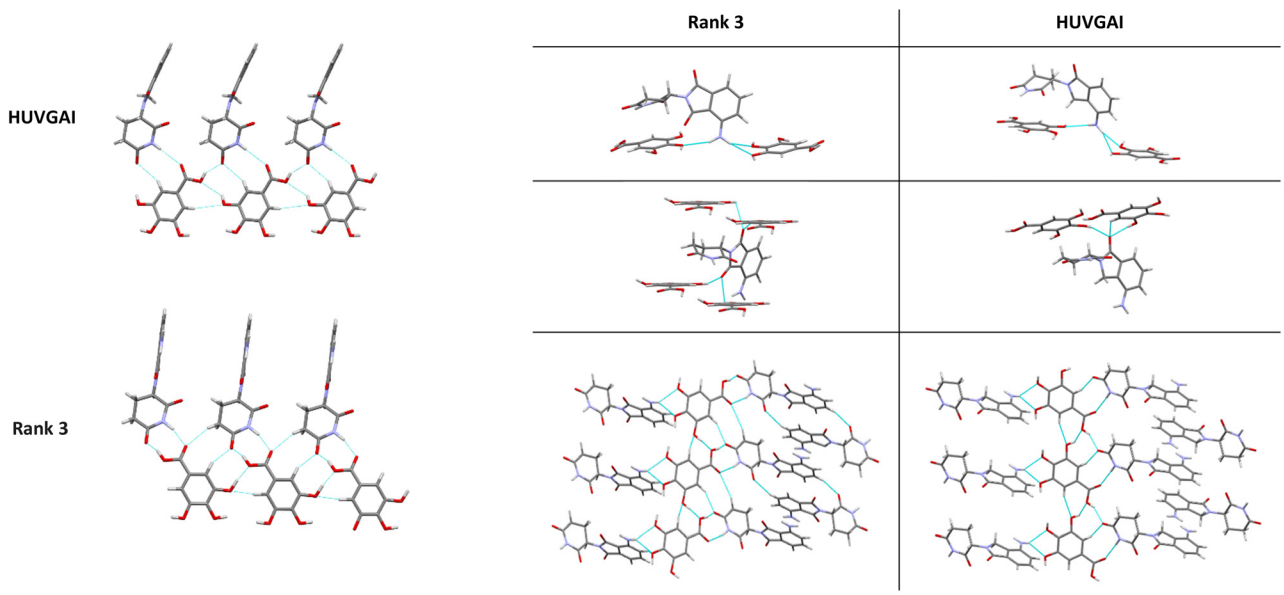

Fig. 9 Synthon interactions for HUVGAI (corresponding lenalidomide co-crystal) and the predicted co-crystal of pomalidomide with gallic acid for ranks 6. Comparison of the HUVGAI co-crystal with rank 6 in terms of interactions involving amine, imide, and carbonyl groups.

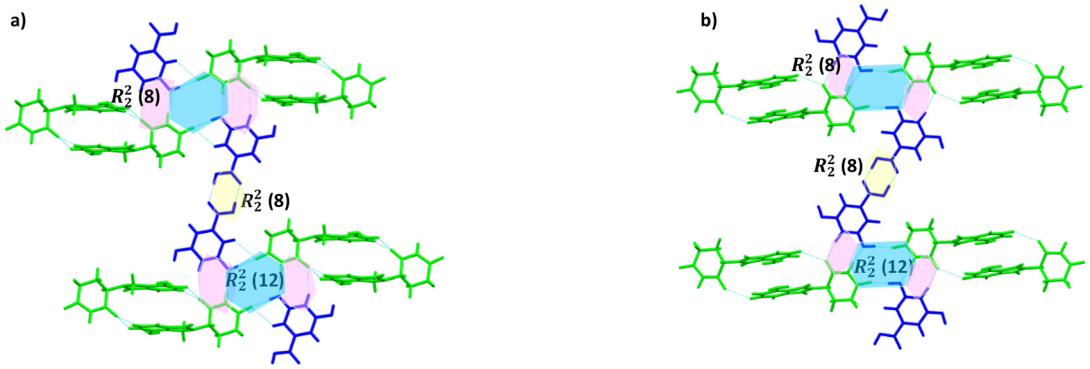

Fig. 10 Illustration of synthon modularity through a comparative analysis of hydrogen bonding patterns between the predicted co-crystal structure ranked 8 and XODPIR. a) Hydrogen bonding arrangement in XODPIR, b) predicted co-crystal structure ranked 1. Both structures feature molecular tetramers composed of two distinct hetero-synthons $R_2^2(8)$ (pink) and $R_2^2(12)$ (blue). These tetramers are interconnected through hydrogen bonding homo-synthons $R_2^2(8)$ (yellow) established between two **DHBA** molecules.

pomalidomide with three selected coformers: urea, gallic acid (GA), and 3,4-dihydroxybenzoic acid (**DHBA**). We successfully identified two polymorphs (forms A and B) and suggested co-crystal structures across several stoichiometric ratios. For polymorphs, lattice energy was used to rank the structures. For co-crystals, Gibbs free energies of formation were calculated, and convex hull analysis was applied to evaluate thermodynamic stability, using the d_h parameter to rank the most stable forms. In addition to energy-based ranking, we applied the concept of synthon modularity as a supporting tool throughout the prediction process. By comparing predicted structures with known synthons observed in thalidomide and lenalidomide, we identified recurring hydrogen-bonding motifs such as N–H···O and C–H···O. These comparisons helped us focus on likely structures, especially when energy differences between candidates were small. We recognize that accurate energy calculations—particularly using DFT and phonon corrections—are the foundation of reliable **CSP**, as confirmed by recent blind tests.[67] However, such methods do not always place the experimental structure among the top-ranked forms and may overlook relevant structures due to small energy differences or conformational complexity. In such cases, chemical insight from crystal engineering concepts like synthon modularity can offer helpful guidance. In conclusion, our results suggest that synthon modularity can assist structure selection in **CSP**, especially when used alongside energy-based methods. It helps highlight likely structures—particularly when prior knowledge of related crystal forms is available.

Data availability

The data supporting this article have been included as part of the ESI.†

Author contributions

We strongly encourage authors to include author contributions and recommend using CRediT for standardised contribution descriptions. Please refer to our general author guidelines for more information about authorship.

Conflicts of interest

There are no conflicts of interest to declare.

Acknowledgements

Z. M. A. and A. S. respectfully acknowledge the Ferdowsi University of Mashhad, Research Council for the financial support of the project Code Number 3/47255. Z. M. A. thanks Skoltech for postdoc fellowship. The authors thank the Cambridge Crystallographic Data Centre for the access to the **CSD** Enterprise. Work of A. R. O. was supported by Russian Science Foundation (grant 19-72-30043).

Notes and references

1 A. R. Oganov, *Modern methods of crystal structure prediction*, John Wiley & Sons, 2011.
2 Z. N. Baghan, A. Salimi, H. Eshtiagh-Hosseini and A. G. Oliver, Hydrogen bond synthons affect the coordination geometry of d^{10}-metal halide complexes: synthetic methods, theoretical studies, and supramolecular architectures, *CrystEngComm*, 2021, **23**, 6276–6290.
3 Z. N. Baghan, A. Salimi, H. Eshtiagh-Hosseini and A. G. Oliver, Hydrogen-bonded 3D network of d 10-metal halide coordination polymer containing N-(3-pyridinyl) nicotinamide: influence of ligand conformation, halide anions and solvent, *CrystEngComm*, 2019, **21**, 2691–2701.
4 D. H. Bowskill, I. J. Sugden, S. Konstantinopoulos, C. S. Adjiman and C. C. Pantelides, Crystal structure prediction methods for organic molecules: State of the art, *Annu. Rev. Chem. Biomol. Eng.*, 2021, **12**, 593–623.
5 C. Greenwell and G. J. Beran, Inaccurate conformational energies still hinder crystal structure prediction in flexible organic molecules, *Cryst. Growth Des.*, 2020, **20**, 4875–4881.
6 Z. M. Abardeh, A. Salimi and A. R. Oganov, Crystal structure prediction of N-halide phthalimide compounds: halogen

bonding synthons as a touchstone, *CrystEngComm*, 2022, **24**, 6066–6075.
7 C. Guo, S. Yin and Y. Wang, Influences of electrostatic models on organic crystal structure prediction–a case study of pentacene, *CrystEngComm*, 2022, **24**, 8477–8487.
8 Q. Zhu and S. Hattori, Organic crystal structure prediction and its application to materials design, *J. Mater. Res.*, 2023, **38**, 19–36.
9 J. Nyman, L. Yu and S. M. Reutzel-Edens, Accuracy and reproducibility in crystal structure prediction: the curious case of ROY, *CrystEngComm*, 2019, **21**, 2080–2088.
10 C. M. Widdifield, H. Robson and P. Hodgkinson, Furosemide's one little hydrogen atom: NMR crystallography structure verification of powdered molecular organics, *Chem. Commun.*, 2016, **52**, 6685–6688.
11 E. Salager, G. M. Day, R. S. Stein, C. J. Pickard, B. Elena and L. Emsley, Powder crystallography by combined crystal structure prediction and high-resolution 1H solid-state NMR spectroscopy, *J. Am. Chem. Soc.*, 2010, **132**, 2564–2566.
12 M. Baias, J.-N. Dumez, P. H. Svensson, S. Schantz, G. M. Day and L. Emsley, De novo determination of the crystal structure of a large drug molecule by crystal structure prediction-based powder NMR crystallography, *J. Am. Chem. Soc.*, 2013, **135**, 17501–17507.
13 A. Jeziorna, P. Paluch, J. Zając, R. Dolot and M. K. Dudek, Crystallization of Elusive Polymorphs of Meloxicam Informed by Crystal Structure Prediction, *Cryst. Growth Des.*, 2023, **23**, 5998–6010.
14 X. Li, X. Ou, B. Wang, H. Rong, B. Wang, C. Chang, B. Shi, L. Yu and M. Lu, Rich polymorphism in nicotinamide revealed by melt crystallization and crystal structure prediction, *Commun. Chem.*, 2020, **3**, 152.
15 C. Yao, I. A. Guzei, Y. Jin, S. Ruan, G. Sun, Y. Gui, L. Wang and L. Yu, Polymorphism of piroxicam: new polymorphs by melt crystallization and crystal structure prediction, *Cryst. Growth Des.*, 2020, **20**, 7874–7881.
16 R. M. Bhardwaj, J. A. McMahon, J. Nyman, L. S. Price, S. Konar, I. D. Oswald, C. R. Pulham, S. L. Price and S. M. Reutzel-Edens, A prolific solvate former, galunisertib, under the pressure of crystal structure prediction, produces ten diverse polymorphs, *J. Am. Chem. Soc.*, 2019, **141**, 13887–13897.
17 A. G. Shtukenberg, Q. Zhu, D. J. Carter, L. Vogt, J. Hoja, E. Schneider, H. Song, B. Pokroy, I. Polishchuk and A. Tkatchenko, Powder diffraction and crystal structure prediction identify four new coumarin polymorphs, *Chem. Sci.*, 2017, **8**, 4926–4940.
18 A. Dey, N. N. Pati and G. R. Desiraju, Crystal structure prediction with the supramolecular synthon approach: Experimental structures of 2-amino-4-ethylphenol and 3-amino-2-naphthol and comparison with prediction, *CrystEngComm*, 2006, **8**, 751–755.
19 J. E. Carpenter and M. Grünwald, Pre-nucleation clusters predict crystal structures in models of chiral molecules, *J. Am. Chem. Soc.*, 2021, **143**, 21580–21593.
20 R. Montis, R. J. Davey, S. E. Wright, G. R. Woollam and A. J. Cruz-Cabeza, Transforming computed energy landscapes into experimental realities: the role of structural rugosity, *Angew. Chem.*, 2020, **132**, 20537–20540.
21 G. R. Desiraju, Crystal engineering: a holistic view, *Angew. Chem., Int. Ed.*, 2007, **46**, 8342–8356.
22 A. Chanan-Khan, A. Swaika, A. Paulus, S. Kumar, J. Mikhael, S. Rajkumar, A. Dispenzieri and M. Lacy, Pomalidomide: the new immunomodulatory agent for the treatment of multiple myeloma, *Blood Cancer J.*, 2013, **3**, e143.
23 G. Fouquet, C. Bories, S. Guidez, L. Renaud, C. Herbaux, S. Javed, T. Facon and X. Leleu, Pomalidomide for multiple myeloma, *Expert Rev. Hematol.*, 2014, **7**, 719–731.
24 S. Semochkin, Pomalidomide in the management of relapsed/refractory multiple myeloma: A review, *Xiandai Zhongliu Yixue*, 2023, **25**, 159–167.
25 R. Rios-Tamayo, A. Martín-García, C. Alarcón-Payer, D. Sánchez-Rodríguez, A. M. D. V. D. de la Guardia, C. G. G. Collado, A. J. Morales, M. J. Chacón and J. C. Barrera, Pomalidomide in the treatment of multiple myeloma: design, development and place in therapy, *Drug Des., Dev. Ther.*, 2017, 2399–2408.
26 G. J. Beran, Frontiers of molecular crystal structure prediction for pharmaceuticals and functional organic materials, *Chem. Sci.*, 2023, **14**, 13290–13312.
27 S. L. Price, Predicting crystal structures of organic compounds, *Chem. Soc. Rev.*, 2014, **43**, 2098–2111.
28 S. L. Price, Why don't we find more polymorphs?, *Acta Crystallogr., Sect. B: Struct. Sci., Cryst. Eng. Mater.*, 2013, **69**, 313–328.
29 H. R. Khavasi, F. Norouzi and A. Azhdari Tehrani, Halogen bonding synthon modularity in coordination compounds, *Cryst. Growth Des.*, 2015, **15**, 2579–2583.
30 S. Tothadi and G. R. Desiraju, Synthon modularity in 4-hydroxybenzamide–dicarboxylic acid cocrystals, *Cryst. Growth Des.*, 2012, **12**, 6188–6198.
31 M. C. Etter, Encoding and decoding hydrogen-bond patterns of organic compounds, *Acc. Chem. Res.*, 1990, **23**, 120–126.
32 J. Bernstein, R. E. Davis, L. Shimoni and N.-L. Chang, Patterns in hydrogen bonding: functionality and graph set analysis in crystals, *Angew. Chem., Int. Ed. Engl.*, 1995, **34**, 1555–1573.
33 G. Bolla, B. Sarma and A. K. Nangia, Crystal engineering of pharmaceutical cocrystals in the discovery and development of improved drugs, *Chem. Rev.*, 2022, **122**, 11514–11603.
34 N. Blagden, M. de Matas, P. T. Gavan and P. York, Crystal engineering of active pharmaceutical ingredients to improve solubility and dissolution rates, *Adv. Drug Delivery Rev.*, 2007, **59**, 617–630.
35 S. N. Wong, Y. C. S. Chen, B. Xuan, C. C. Sun and S. F. Chow, Cocrystal engineering of pharmaceutical solids: Therapeutic potential and challenges, *CrystEngComm*, 2021, **23**, 7005–7038.
36 J. W. Steed, The role of co-crystals in pharmaceutical design, *Trends Pharmacol. Sci.*, 2013, **34**, 185–193.
37 J. B. Ngilirabanga and H. Samsodien, Pharmaceutical co-crystal: An alternative strategy for enhanced physicochemical properties and drug synergy, *Nano Sel.*, 2021, **2**, 512–526.

38 T. S. Thakur and G. R. Desiraju, Crystal structure prediction of a Co-crystal using a supramolecular synthon approach: 2-methylbenzoic acid– 2-amino-4-methylpyrimidine, *Cryst. Growth Des.*, 2008, **8**, 4031–4044.
39 X. Liu, H. Niu and A. R. Oganov, COPEX: co-evolutionary crystal structure prediction algorithm for complex systems, *npj Comput. Mater.*, 2021, **7**, 199.
40 A. R. Oganov, C. J. Pickard, Q. Zhu and R. J. Needs, Structure prediction drives materials discovery, *Nat. Rev. Mater.*, 2019, **4**, 331–348.
41 M. Frisch, G. Trucks, H. Schlegel, G. Scuseria, M. Robb, J. Cheeseman, G. Scalmani, V. Barone, B. Mennucci and G. Petersson, Uranyl extraction by N, N-dialkylamide ligands studied by static and dynamic DFT simulations, *Gaussian*, 2009, vol. 9, p. 227.
42 Q. Zhu, A. R. Oganov, C. W. Glass and H. T. Stokes, Constrained evolutionary algorithm for structure prediction of molecular crystals: methodology and applications, *Acta Crystallogr., Sect. B: Struct. Sci.*, 2012, **68**, 215–226.
43 A. O. Lyakhov, A. R. Oganov, H. T. Stokes and Q. Zhu, New developments in evolutionary structure prediction algorithm USPEX, *Comput. Phys. Commun.*, 2013, **184**, 1172–1182.
44 A. R. Oganov and C. W. Glass, Crystal structure prediction using ab initio evolutionary techniques: Principles and applications, *J. Chem. Phys.*, 2006, **124**, 244704.
45 A. R. Oganov, A. O. Lyakhov and M. Valle, How Evolutionary Crystal Structure Prediction Works and Why, *Acc. Chem. Res.*, 2011, **44**, 227–237.
46 S. L. Mayo, B. D. Olafson and W. A. Goddard, DREIDING: a generic force field for molecular simulations, *J. Phys. Chem.*, 1990, **94**, 8897–8909.
47 A. K. Rappe and W. A. Goddard III, Charge equilibration for molecular dynamics simulations, *J. Phys. Chem.*, 1991, **95**, 3358–3363.
48 J. D. Gale and A. L. Rohl, The general utility lattice program (GULP), *Mol. Simul.*, 2003, **29**, 291–341.
49 J. A. Chisholm and S. Motherwell, COMPACK: a program for identifying crystal structure similarity using distances, *J. Appl. Crystallogr.*, 2005, **38**, 228–231.
50 S. Grimme, J. Antony, S. Ehrlich and H. Krieg, A consistent and accurate ab initio parametrization of density functional dispersion correction (DFT-D) for the 94 elements H-Pu, *J. Chem. Phys.*, 2010, **132**, 154104.
51 G. Kresse and J. Furthmüller, Efficient iterative schemes for ab initio total-energy calculations using a plane-wave basis set, *Phys. Rev. B: Condens. Matter Mater. Phys.*, 1996, **54**, 11169.
52 G. Kresse and J. Hafner, Ab initio molecular dynamics for liquid metals, *Phys. Rev. B: Condens. Matter Mater. Phys.*, 1993, **47**, 558.
53 G. Kresse and J. Hafner, Ab initio molecular-dynamics simulation of the liquid-metal–amorphous-semiconductor transition in germanium, *Phys. Rev. B: Condens. Matter Mater. Phys.*, 1994, **49**, 14251.
54 P. E. Blöchl, Projector augmented-wave method, *Phys. Rev. B: Condens. Matter Mater. Phys.*, 1994, **50**, 17953.
55 G. Kresse and D. Joubert, From ultrasoft pseudopotentials to the projector augmented-wave method, *Phys. Rev. B: Condens. Matter Mater. Phys.*, 1999, **59**, 1758.
56 J. D. Gale, L. M. LeBlanc, P. R. Spackman, A. Silvestri and P. Raiteri, *J. Chem. Theory Comput.*, 2021, **17**, 7827–7849.
57 K. Ravikumar and B. Sridhar, Lenalidomide, an antineoplastic drug, and its hemihydrate, *Acta Crystallogr., Sect. C: Cryst. Struct. Commun.*, 2009, **65**, o502–o505.
58 R. Chennuru, P. Muthudoss, R. S. Voguri, S. Ramakrishnan, P. Vishweshwar, R. R. C. Babu and S. Mahapatra, Iso-structurality induced solid phase transformations: a case study with lenalidomide, *Cryst. Growth Des.*, 2017, **17**, 612–628.
59 J.-X. Song, Y. Yan, J. Yao, J.-M. Chen and T.-B. Lu, Improving the solubility of lenalidomide via cocrystals, *Cryst. Growth Des.*, 2014, **14**, 3069–3077.
60 J.-X. Song, J.-M. Chen and T.-B. Lu, Lenalidomide–gallic acid cocrystals with constant high solubility, *Cryst. Growth Des.*, 2015, **15**, 4869–4875.
61 J. C. Reepmeyer, M. O. Rhodes, D. C. Cox and J. V. Silverton, Characterization and crystal structure of two polymorphic forms of racemic thalidomide, *J. Chem. Soc., Perkin Trans. 2*, 1994, 2063–2067.
62 F. Allen and J. Trotter, Crystal and molecular structure of thalidomide, N-(α-glutarimido)-phthalimide, *J. Chem. Soc. B*, 1971, 1073–1079.
63 M. Caira, S. Botha and D. Flanagan, Polymorphism of N-(2, 6-dioxo-3-piperidyl) pthalimide (thalidomide): structural characterization of a second monoclinic racemic modification, *J. Chem. Crystallogr.*, 1994, **24**, 95–99.
64 T. Suzuki, M. Tanaka, M. Shiro, N. Shibata, T. Osaka and T. Asahi, Evaluation of stability difference between asymmetric homochiral dimer in (S)-thalidomide crystal and symmetric heterochiral dimer in (RS)-thalidomide crystal, *Phase Transitions*, 2010, **83**, 223–234.
65 G. P. Stahly, D. Jonaitis, H.-W. Hui and K. J. Klopfer, *US Pat.*, 9974780, 2018; B. M. Cohen, Y. Li, J. Xu, W. W. Leong and H. Man, *WO Pat.*, 2013/126326, 2013.
66 S. Habermehl, P. Moerschel, P. Eisenbrandt, S. M. Hammer and M. U. Schmidt, *Acta Crystallogr., Sect. B: Struct. Sci., Cryst. Eng. Mater.*, 2014, **70**, 347–359.
67 L. M. Hunnisett, J. Nyman, N. Francia, N. S. Abraham, C. S. Adjiman, S. Aitipamula, T. Alkhidir, M. Almehairbi, A. Anelli, D. M. Anstine, J. E. Anthony, J. E. Arnold, F. Bahrami, M. A. Bellucci, R. M. Bhardwaj, I. Bier, J. A. Bis, A. D. Boese, D. H. Bowskill, J. Bramley, J. G. Brandenburg, D. E. Braun, P. W. V. Butler, J. Cadden, S. Carino, E. J. Chan, C. Chang, B. Cheng, S. M. Clarke, S. J. Coles, R. I. Cooper, R. Couch, R. Cuadrado, T. Darden, G. M. Day, H. Dietrich, Y. Ding, A. DiPasquale, B. Dhokale, B. P. van Eijck, M. R. J. Elsegood, D. Firaha, W. Fu, K. Fukuzawa, J. Glover, H. Goto, C. Greenwell, R. Guo, J. Harter, J. Helfferich, D. W. M. Hofmann, J. Hoja, J. Hone, R. Hong, G. Hutchison, Y. Ikabata, O. Isayev, O. Ishaque, V. Jain, Y. Jin, A. Jing, E. R. Johnson, I. Jones, K. V. J. Jose, E. A. Kabova, A. Keates, P. F. Kelly, D. Khakimov, S. Konstantinopoulos, L. N. Kuleshova, H. Li, X.

Lin, A. List, C. Liu, Y. M. Liu, Z. Liu, Z.-P. Liu, J. W. Lubach, N. Marom, A. A. Maryewski, H. Matsui, A. Mattei, R. A. Mayo, J. W. Melkumov, S. Mohamed, Z. M. Abardeh, H. S. Muddana, N. Nakayama, K. S. Nayal, M. A. Neumann, R. Nikhar, S. Obata, D. O'Connor, A. R. Oganov, K. Okuwaki, A. Otero-de-la-Roza, C. C. Pantelides, S. Parkin, C. J. Pickard, L. Pilia, T. Pivina, R. Podeszwa, A. J. A. Price, L. S. Price, S. L. Price, M. R. Probert, A. Pulido, G. R. Ramteke, A. U. Rehman, S. M. Reutzel-Edens, J. Rogal, M. J. Ross, A. F. Rumson, G. Sadiq, Z. M. Saeed, A. Salimi, M. Salvalaglio, L. S. de Almada, K. Sasikumar, S. Sekharan, C. Shang, K. Shankland, K. Shinohara, B. Shi, X. Shi, A. G. Skillman, H. Song, N. Strasser, J. van de Streek, I. J. Sugden, G. Sun, K. Szalewicz, B. I. Tan, L. Tan, F. Tarczynski, C. R. Taylor, A. Tkatchenko, R. Tom, M. E. Tuckerman, Y. Utsumi, L. Vogt-Maranto, J. Weatherston, L. J. Wilkinson, R. D. Willacy, L. Wojtas, G. R. Woollam, Z. Yang, E. Yonemochi, X. Yue, Q. Zeng, Y. Zhang, T. Zhou, Y. Zhou, R. Zubatyuk and J. C. Cole, *Acta Crystallogr., Sect. B: Struct. Sci., Cryst. Eng. Mater.*, 2024, **80**, 517–547.